Computation of Hypersonic Flow Through A Narrow Expansion Slot

Ching-Mao Hung* and Timothy J. Barth†
NASA Ames Research Center, Moffett Field, California

The compressible Navier-Stokes equations are numerically solved for hypersonic flow over a three-dimensional ramp with a narrow expansion slot. In a two-dimensional test case, it is shown that a higher-order scheme is needed to avoid excessive numerical dissipation and hence too much total-pressure loss. The calculation demonstrates the role of viscosity in the expansion process of hypersonic flow through the narrow slot. Cases with various wall temperatures and slot widths are studied. Calculations show that wall cooling reduces the thickness of boundary layer and hence increases the flow expansion substantially. In the lower portion of the slot, inviscidly, the flow is dominated by a highly expanded low-density fluid, and viscously, by a viscous layer. As a direct consequence, as soon as the wedge angle is large enough, the mass flux through the slot is almost constant.

I. Introduction

IN the development of a hypersonic vehicle, design of the propulsion system is one of the most important engineering problems. A supersonic combustion ramjet (a.k.a. scramjet) is a popular candidate. This design is not without its problems. In the hypersonic flow regime it is relatively easy, through high-speed compression, to obtain a condition of high pressure and temperature desired for combustion. However, a hypersonic shear layer tends to be very stable and optimal scramjet performance requires that the flow provides good mixing characteristics within a reasonable downstream distance for supersonic combustion. Therefore, a fuel injection system with enhanced mixing is of great interest to the design engineer. Various fuel injection systems have been investigated for different speed ranges and flow conditions.[1] Figure 1 shows a representative generic mixed-cycle scramjet engine. Note that this particular design utilizes three types of fuel injection systems depending on the flow conditions: retractable axial injectors ($M \lesssim 3$), wall injectors ($M \lesssim 7$), and axial slot injectors ($M \gtrsim 7$). At low supersonic speeds, the retractable axial injectors and wall injectors are used. As the speed increases, the retractable injectors would retract first, and then eventually the wall injector would be turned off. This prevents thermal overloading on the walls in the vicinity of the injector and reduces total pressure losses. At this point ($M \gtrsim 7$), axial slot injectors are used to introduce fuel into the flowing air. In the remainder of this paper, we will numerically study flowfield characteristics for a simplified model of an axial slot injector. Figure 2 shows our generic model of an axial slot injector, which consists of a three-dimensional compression ramp with narrow expansion slot. In the actual device, the fuel is axially injected at the end of the compression ramp (not modeled in this study). The expansion slot is designed to induce high-speed fluid through the slot to mix air with the injected fuel side-by-side. This system has several advantages:

1) The side-by-side air-fuel mixing increases the air-fuel contact surface and ideally is devised to trigger the instability of the air-fuel shear layer.

2) The streamwise injection alleviates the problem of high stagnation heat and high total pressure loss associated with wall injection and hence is suitable for high Mach number range conditions.

One main question is the effectiveness of the narrow expansion slot. Recall that in hypersonic flow over a convex corner, streamtubes will increase drastically in cross-sectional area. (For instance, when inviscid air adiabatically expands from Mach 5 to Mach 7, its streamtube area increases about 4.17 times.) This compounds the viscous layer thickening so much that the effectiveness of flow expansion is substantially reduced. This degradation is further aggravated in a narrow expansion slot due to the close proximity of the three walls. The objective of the present paper is to study the role of viscosity in the expansion process of hypersonic flow through the narrow slot. Since the purpose of this device is to induce high-momentum fluid into the slot, two main concerns to be addressed will be the effect of viscous blockage on the mass flux through the slot and losses in thrust and total pressure. In addition, one should also be concerned about stall or streamwise separation in the expansion slot.

In the present study, the three-dimensional compressible Navier-Stokes equations are solved by a flux-difference splitting code, which is discussed in Section III. Preliminary calculations are first carried out on a two-dimensional expansion corner to assess the effects of numerical errors on the prediction of these flowfields. The most accurate scheme from this test is then used to calculate Mach 4.9 flow over the three-dimensional expansion slot geometry described in Section II. This simple geometry excludes other complications and allows us to concentrate only on the expansion process. The flow is assumed laminar in all calculations. Cases with various wall temperatures and slot width aspect ratios will be investigated. Finally, inviscid results for a compression ramp with a flat slot will also be presented to contrast flowfield characteristics for a flow expanding from the ramp into the slot. The two-dimensional Prandtl-Meyer and three-dimensional inviscid solutions will be used to contrast the role of viscosity in this study. A grid of $65 \times 49 \times 65$ is used for most of the three-dimensional calculations with calculations on a finer grid of $129 \times 97 \times 129$ used to show grid independence.

We note that in the present analysis restrictive assumptions have been made. The flow is assumed to be laminar in all

Presented as Paper 88-0232 at the AIAA 26th Aerospace Sciences Meeting, Reno. NV, Jan. 11-14, 1988; received Jan. 15, 1988; revision received Feb 7, 1989.

*Research Scientist, Computational Fluid Dynamics Branch. Associate Fellow, AIAA.

†Research Scientist, Computational Fluid Dynamics Branch.

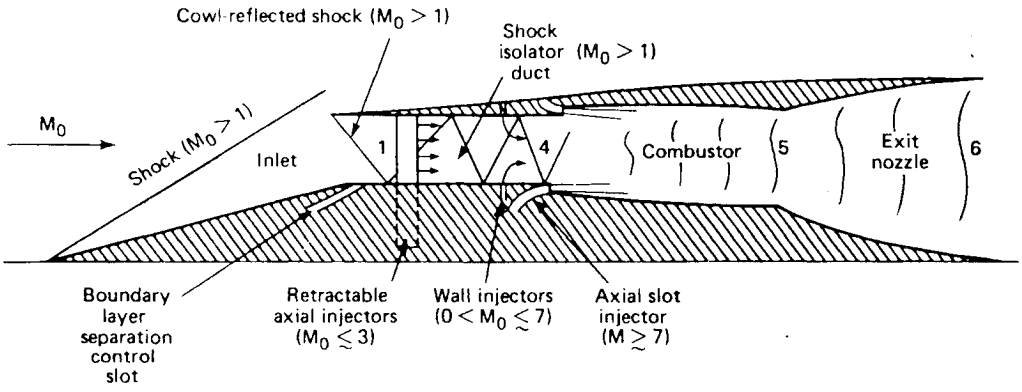

Fig. 1 Representative generic mixed-cycle scramjet engine.

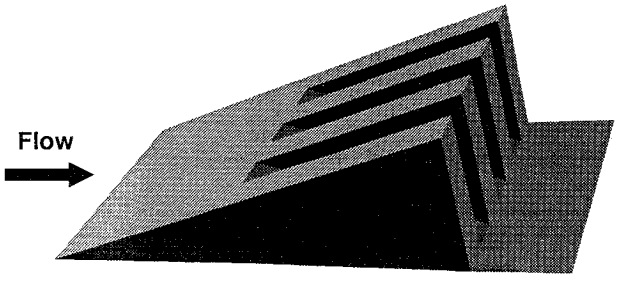

Fig. 2 3-D compression ramp with a narrow slot.

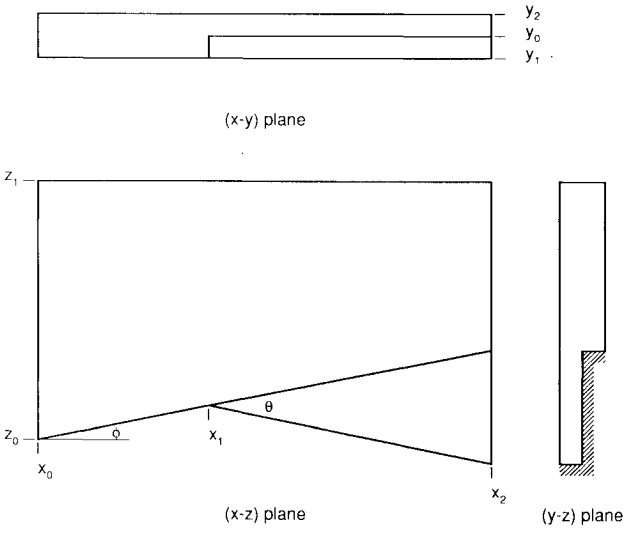

Fig. 3 Schematic plane views of computational domain.

cases. This would be a severe limitation for applying the results directly to a realistic hypersonic vehicle. Also note that the vehicle boundary layer ingested by the fuel injector assembly is not considered. For a hypersonic vehicle with a long ramp, this could significantly affect the flowfield in the region considered. Finally, real gas effects, which are very important at high-flight Mach number, are not included in the present study.

II. Problem Description

The configuration shown in Fig. 2 can be modeled as a periodic array of compression ramps with expansion slots. In reality the geometry may also exhibit top-bottom symmetry in which case only half problem need be solved. Figure 3 shows views of the (x,y), (x,z) and the last (y,z) planes in the domain of computation. Flow is assumed symmetric at $y = y_1$ and $y = y_2$ in the $(x - y)$ plane and at $z = z_1$ in the $(x - z)$ plane. Entering the geometry in the $(x - z)$ plane from left to right, the flow first encounters a compression ramp of angle ϕ at x_0 then expands through a slot of angle θ to the ramp surface at x_1. The dimensions used in the present study are $x_0 = -2.5$, $x_1 = 0.0$, $x_2 = 4.25$, $y_2 - y_0 = 0.25$, $z_0 = 0.0$, and $z_1 = 3.0$. The main results will be presented for an expansion slot case, $\phi = 0$, $\theta = -20$ deg. A compression slot, $\theta = 20$ deg, is also computed to contrast the flow characteristics.

The openness of the slot is characterized by the ratio of slot width to the plate width, i.e., $|y_1 - y_0|/|y_2 - y_0|$. The basic geometries have width ratios of one and two. The term "narrow" adopted in this study is in reference to the high aspect ratio of slot height to slot width. This creates difficulties in generating a single-block, body-fitted grid system. (This is especially true if near orthogonality and grid point clustering are desired.) An interactive hyperbolic grid generator developed by Cordova and Barth[2] was employed to generate the three-dimensional grid as a series two-dimensional $(y - z)$ plane grid. Grids ranging in size from $(65 \times 49 \times 65)$ to $(129 \times 79 \times 129)$ were generated for the present study. Figure 4 shows the surface grid and typical $(y - z)$ plane grid.

III. Numerical Method

The numerical code used is a finite-volume, TVD adaptation of the ARC3D code developed by Pulliam and Steger.[3] The Navier-Stokes equations are solved in conservation law form under the generalized coordinate transformation, $\boldsymbol{r}' = \boldsymbol{r}'(\boldsymbol{r})$ with $\boldsymbol{r} = [x,y,z]^t$,

$$\frac{\partial \boldsymbol{u}}{\partial t} + \sum_{i=1}^{3} \frac{\partial \boldsymbol{f}(\boldsymbol{u})^i}{\partial \boldsymbol{r}'_i} = \sum_{i=1}^{3} \frac{\partial \boldsymbol{v}(\boldsymbol{u})^i}{\partial \boldsymbol{r}'_i}$$

Here $\boldsymbol{u}$ is the vector of conserved variables for mass, momentum, and energy. The vectors $\boldsymbol{f}$ and $\boldsymbol{v}$ are the inviscid and viscous flux vectors, respectively. For a specific description of these vectors, see Ref. 3 for details. The equations are then rewritten in integral form for a finite-volume Ω with its corresponding cell surface boundary $\partial\Omega$;

$$\frac{\partial}{\partial t} \int_{\Omega} \boldsymbol{u} \, dv + \oint_{\partial\Omega} [\bar{\boldsymbol{f}}(\hat{\boldsymbol{n}}) - \bar{\boldsymbol{v}}(\hat{\boldsymbol{n}})] \, ds = 0$$

Here $\bar{f}$ and $\bar{v}$ are the oriented inviscid and viscous fluxes with respect to the outward cell surface normal $(\hat{n})$,

$$\bar{\boldsymbol{f}}(\hat{\boldsymbol{n}}) = \sum_{i=1}^{3} \boldsymbol{n}_{x_i} \boldsymbol{f}^i, \quad \bar{\boldsymbol{v}}(\hat{\boldsymbol{n}}) = \sum_{i=1}^{3} \boldsymbol{n}_{x_i} \boldsymbol{v}^i$$

The surface integral is then approximated by midpoint rule with the resulting sum over all cell face,

$$\oint_{\partial\Omega} [\bar{f}(\hat{n}) - \bar{v}(\hat{n})]\, ds \approx \sum_{j=1}^{\#\text{ faces}} [\bar{f}(u^R, u^L; \hat{n})_j - \bar{v}(\bar{u}, \nabla u; \hat{n})_j] s_j$$

In the present scheme, the numerical viscous fluxes are calculated using symmetric averages for $\bar{u}$ and the usual second-order central differencing for ∇u. The Roe flux function is used for the inviscid fluxes, i.e.,

$$\bar{f}(u^R, u^L; \hat{n}) = \frac{1}{2}[f^i(u^R; \hat{n}) + f^i(u^L; \hat{n})] - \frac{1}{2}|A^i(u^R, u^L; \hat{n})|(u^R - u^L)$$

where $|A|$ is a positive definite matrix formed from the flux Jacobian $\partial f/\partial u$; see Ref. 4 for details. The state variables, u^R and u^L, are obtained using the MUSCL monotone interpolation/extrapolation formulas.[5,6] On a grid with coordinate indices (j,k,l), the interpolation/extrapolation formulas for a cell face on a grid coordinate $(k,l = \text{const})$ would take the form:

$$u^R_{j+1/2} = u_{j+1} - \frac{(1-\kappa)}{4}\,\text{minmod}(\Delta_{j+3/2}u, \beta\Delta_{j+1/2}u) - \frac{(1+\kappa)}{4}\,\text{minmod}(\Delta_{j+1/2}u, \beta\Delta_{j+3/2}u)$$

$$u^L_{j+1/2} = u_j + \frac{1-\kappa}{4}\,\text{minmod}(\Delta_{j-1/2}u, \beta\Delta_{j+1/2}u) + \frac{(1+\kappa)}{4}\,\text{minmod}(\Delta_{j+1/2}u, \beta\Delta_{j-1/2}u)$$

where

$$\text{minmod}(x,y) = \begin{cases} x \text{ if } |x| \le |y| \text{ and } & x \cdot y > 0 \\ y \text{ if } |x| > |y| \text{ and } & x \cdot y > 0 \\ 0 \text{ if } & x \cdot y \le 0 \end{cases}, \quad \beta \le \frac{3-\kappa}{1-\kappa}$$

Depending on the value κ, various second-order accurate schemes can be obtained as well as one third-order scheme ($\kappa = 1/3$) when no limiting is used. For the expansion slot calculations no limiting was used so as to obtain the highest accuracy. For the compression ramp calculations, flux limiting was used with β set to its maximum limit. First-order upwind results are presented for comparison by setting $\beta = 0$, second-order calculations are carried out with $\kappa = -1$ (fully upwind), and third-order calculations with $\kappa = 1/3$.

The ARC3D code assumes a thin-layer form of the equations whereby viscous terms are only retained in one coordinate direction. The wall is assumed impermeable with zero pressure gradient, and tangent or no-slip boundary conditions are applied for either inviscid or viscous flow respectively. For the viscous cases, calculations are performed for both adiabatic and isothermal walls to study the heat transfer effects on the expansion process. A typical three-dimensional flowfield solution, with mesh size of $(65 \times 49 \times 65)$, required about 45 min of CPU time on a CRAY-2 computer.

IV. Results and Discussion

In this section we will present results for calculations performed with a freestream Mach number of 4.90 and Reynolds number of 0.1×10^6 for a 20 deg expansion slot. Results will be first presented in two dimensions in which numerical schemes ranging from first order to third order will be evaluated. Adiabatic wall conditions with zero wall pressure gradient are assumed. Using information from these calculations, three-dimensional results will be presented.

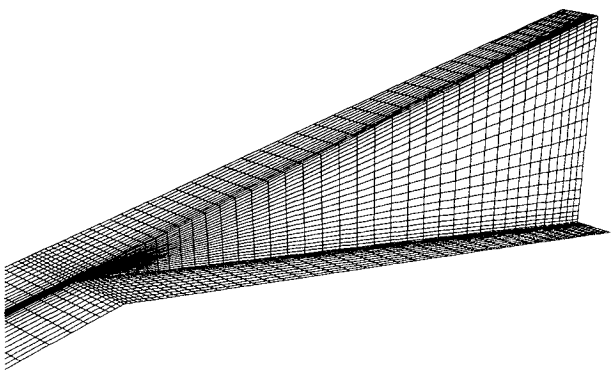

a) Surface grid

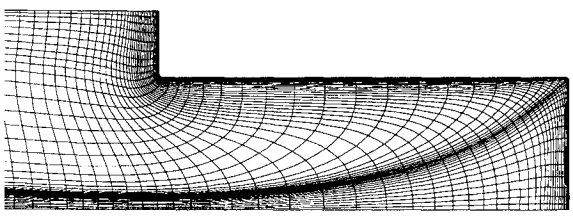

b) Grid in $(y-z)$ plane

Fig. 4 Grid on body surface and $(y-z)$ plane.

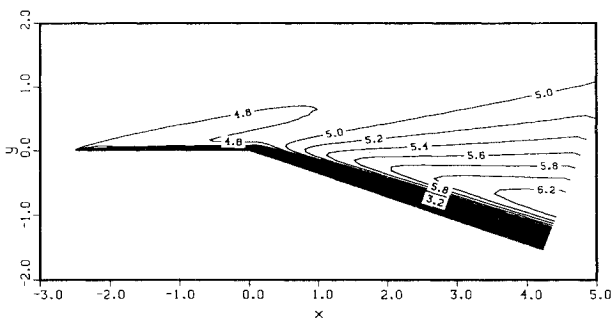

a) First-order

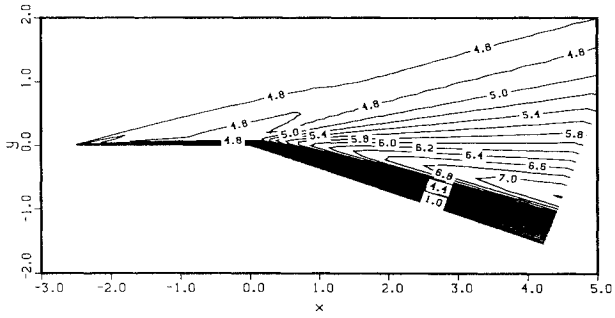

b) Second-order

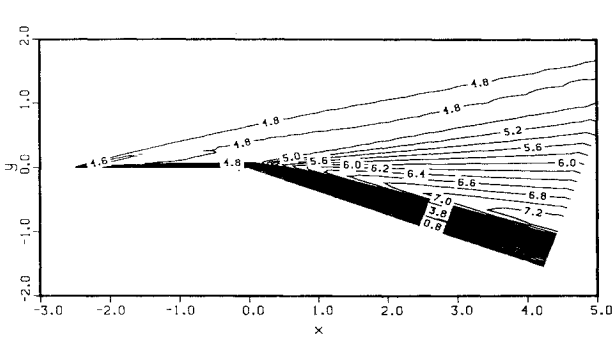

c) Third-order

Fig. 5 Mach contours for three schemes.

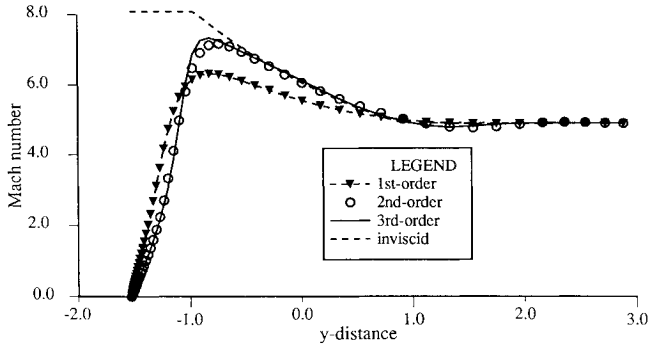

a) Mach number

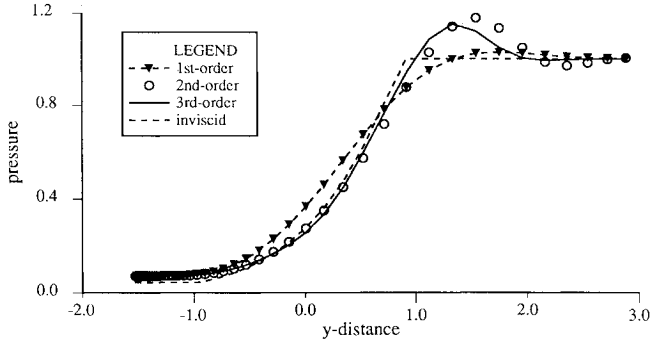

b) Pressure

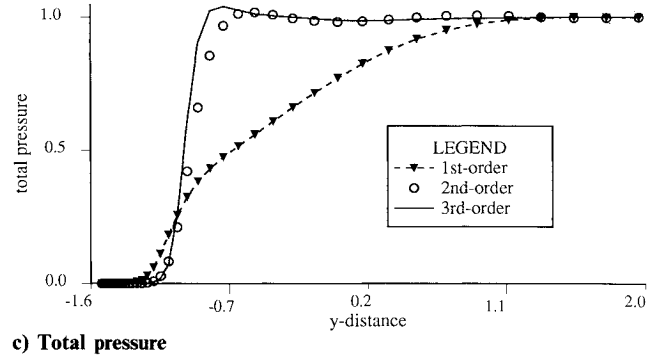

c) Total pressure

Fig. 6 Comparison of profiles at $x = 4.2$

Figures 5a-5c show the calculated Mach number contour plots for two-dimensional 20-deg expansion corner using the first-, second-, and third-order schemes respectively on a (256×65) grid. (The y-coordinate used in two dimensions is equivalent to the z-coordinate in the three-dimensional geometry shown in Fig. 4.) In these flows the incoming flow is uniform ($M = 4.9$). This produces a weak leading-edge shock that should exit at the downstream boundary. Note that all schemes predict a substantial thickening of the viscous layer as the flow turns through the expansion corner. The first-order scheme smooths out the expansion fan considerably and the leading edge shock is dissipated before it reaches the downstream boundary. The second- and third-order solutions (Figs. 5b and 5c) have a substantially stronger expansion wave and a leading-edge shock that extends to the downstream boundary. Figures 6a-6c compare the calculated results of Mach number, pressure, and total pressure at $x = 4.2$ using the first-, second, and third-order schemes as well as the inviscid Prandtl-Meyer solution at this location. Note that the presence of a leading-edge shock produces a pressure peak at $y \approx 1.35$ which is not modeled in the Prandtl-Meyer solution. Again, the effect of numerical dissipation present in the first-order solution is clear. The pressure peak resulting from the leading-edge shock (Fig. 6b) is smoothed out, and the

Table 1 2-D calculated results at $x = 4.2$

	1st order	2nd order	3rd order	Inviscid
p/p_∞ min	0.0611	0.0728	0.0706	0.0450
$p_t/p_{t\infty}$ max	1.0007	1.0876	1.0539	1.000
Mach No. max	6.35	7.21	7.36	8.08
Effective Angle	11.3°	16.0°	16.8°	20.0°
T_w/T_∞	2.915	3.973	4.113	(5.075)
mass flux	0.1801	0.1720	0.1706	0.1863
p_t loss	0.605	0.383	0.350	.0

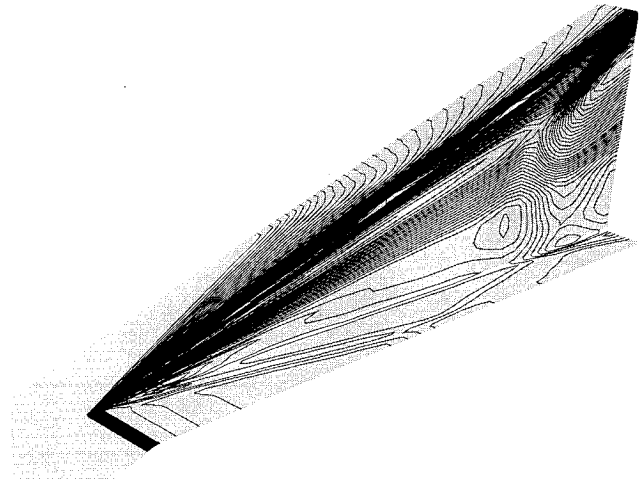

Fig. 7 Surface density contours (inviscid).

expanded Mach number (Fig. 6a) is substantially underpredicted. The improvement of the high-order schemes is clearly demonstrated in the total pressure, p_t, plots. For idealized air at high Mach number, p_t/p is proportional to M^7; a slight underprediction of Mach number results in a severe underprediction in total pressure. The local Mach number computed using the second-order and third-order schemes follows the 2-D inviscid solution closely for $y \geq -0.83$ with almost no total pressure loss. Approaching the viscous layer, the Mach number deviates from the inviscid solution, and the total pressure decreases drastically. (The location of this drop in total pressure is a good indication of the edge of the viscous layer.) Table 1 shows a summary of flow properties predicted by the three different schemes. The mass flux and loss of total pressure are defined as an integration of the corresponding properties from the bottom of the expansion wedge to the level of plate at a given x-location and normalized by freestream value. (In the present case, $x = 4.2$ and the integration is from $y = -x \tan 20$ deg to $y = 0$.) The predicted maximum Mach numbers are 6.35, 7.21, and 7.36, and with corresponding effective wedge angles of 11.3 deg, 16 deg, and 16.8 deg, respectively. The first-order scheme predicts a 60% total pressure loss whereas the third-order scheme predicts only about a 35% loss. It is interesting to note that even though roughtly 35% of the expansion wedge is dominated by the viscous layer, the mass flux is not that much different from the inviscid result. (Details of this will be discussed later.) Treated adiabatically, the wall temperatures at $x = 4.2$ are $T_w/T_\infty = 2.92$, 3.97, and 4.11 for the three different schemes, respectively. (The laminar adiabatic wall temperature based on the inflow condition is $T_{aw}/T_\infty = 5.08$.) From these calculations, the importance of reducing numerical viscosity is apparent. For the remaining three-dimensional calculations, the third-order scheme will be used exclusively. A three-dimensional inviscid solution is first obtained for comparing the effects of viscosity. The density contours on the body surface ($l = 1$) are shown in Fig. 7. Note that a wave (a compression wave with respect to the slot) is generated by the flow expansion around the axial corner, which eventually impinges

on the wall on the opposite side of the slot. This causes a pressure and density increase in the slot after the Prandtl-Meyer expansion. In one way, this helps to induce fluid into the slot but may lead to flow separation due to the adverse pressure gradient generated in the slot (see later discussions).

Next, three-dimensional viscous calculations are carried out for the expansion slot (plate to slot to width ratio equal to one) with adiabatic wall conditions using a $65 \times 49 \times 65$ grid. The Mach number and total pressure are shown in Figs. 8a–b for the center plane of the slot ($k = 1$). Again note that a weak leading-edge shock is present that travels out the downstream boundary of the domain. The total pressure contours indicate that the viscous layer is very thick downstream of the corner as was seen in the two-dimensional case.

This case was also computed on a grid refined in all directions ($129 \times 97 \times 129$). Comparison of pressure contours along the slot central plane is shown in Figs. 9a–b. These plots indicate some improvement in wave resolution, most notably the leading-edge shock with a minor improvement in the expansion wave generated from the corner. Nevertheless, all the main features appear to be present in the ($65 \times 49 \times 65$) grid calculations. Plots of Mach number contours at several ($y - z$) planes are presented in Fig. 10 for the standard grid. Roughly 75% of the slot is essentially dominated by a viscous layer of constant pressure and low total pressure fluid. (Care should be taken, as the thickness of the viscous layer is also strongly dependent on the magnitude of expansion angle.) The viscous layer along the vertical slot wall is also very thick. From Fig. 10 it appears that up to the length of the computed domain, the boundary layer has not fully developed in the slot.

In hypersonic flow, an adiabatic wall leads to very high wall temperatures. In a narrow slot, fluid will be heated by hot walls on three sides. This has a pronounced effect on the flow expansion process. Figure 11 shows Mach number contours at several ($y - z$) planes for the narrow slot calculated with wall cooling. The wall is assumed isothermal with the wall temperature equal to 40% of stagnation temperature. The thickness of the viscous layer is significantly reduced. The width of the slot opening affects the blockage due to viscosity, and the sensitivity of slot width is investigated in the next calculation. A case with slot width ratio $|y_1 - y_0|/|y_2 - y_0| = 2.0$ was computed, and Mach number contours are displayed in Fig. 12. In the following paragraphs these calculations will be quantitatively compared.

From the above calculations, we observe that viscosity plays an important role in the expansion process of hypersonic flow through a narrow slot. Various wall conditions and slot widths have significant effects on the flow structures. To have a detailed comparison of the entire flowfield would be impossible. Here, we use the profiles of Mach number, pressure, and total pressure along the centerline of the slot at the exit plane (Figs 13a–c) to give a simple quantitative comparison for various three-dimensional conditions discussed above. The two-dimensional viscous solution is also included in the graphs for comparison. The bottom of the slot is located at about $z = -1.54$. Shown in Fig. 13a, for a large portion of the slot, the Mach number for the three-dimensional adiabatic-wall narrow slot case (width ratio of one) is much lower than the two-dimensional viscous solution. The Mach number for the isothermal and the wide slot cases shows substantial improvements toward the value of the two-dimensional viscous result. These viscous effects due to a narrow slot are also clearly shown in the pressure and total pressure plots, Figs. 13b and c.

Table 2 summarizes the predicted results and their integrated properties at the exit plane for all the calculated cases. (Here the mass flux and total pressure loss are their values integrated over the exit plane of the slot gap, $z \leq 0.0$.) For the adiabatic narrow-slot case, more than 75% of the slot is dominated by the viscous layer, which produces a 74% total pressure loss, compared to only 35% for the two-dimensional case. The isothermal and wide-slot cases have about a 60% loss in total pressure. The maximum Mach number of the adiabatic case only reaches a maximum of 6.05, equivalent to an effective wedge angle of 9.06 deg.

One interesting characteristic of these flows is the relative insensitivity of mass flux through the slot gap, even though the viscous layer is very thick and is strongly affected by wall temperature and slot width. To understand this, consider

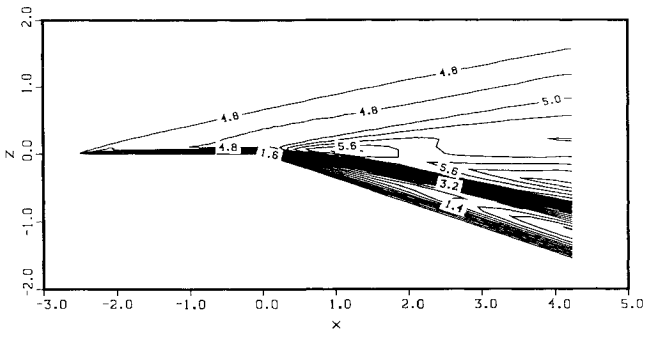

a) Center plane Mach contours

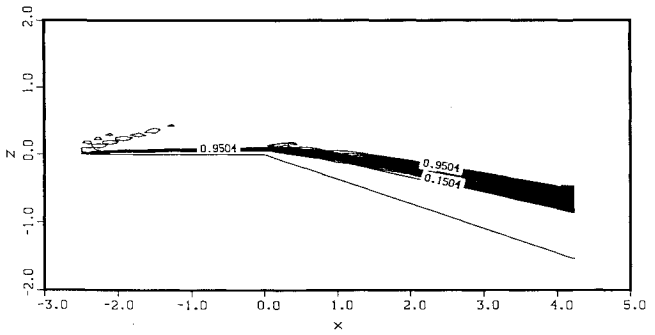

b) Center plane total pressure contours

Fig. 8 Three-dimensional viscous expansion slot.

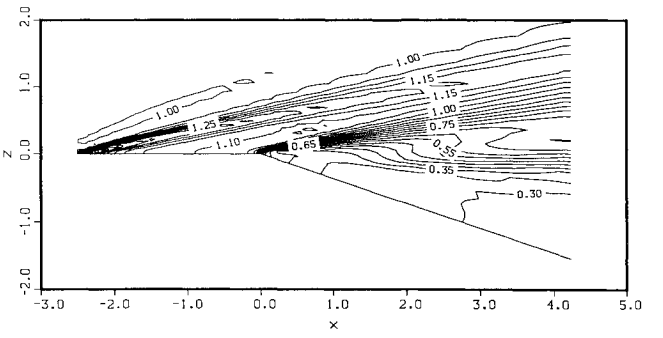

a) Standard grid ($65 \times 49 \times 65$)

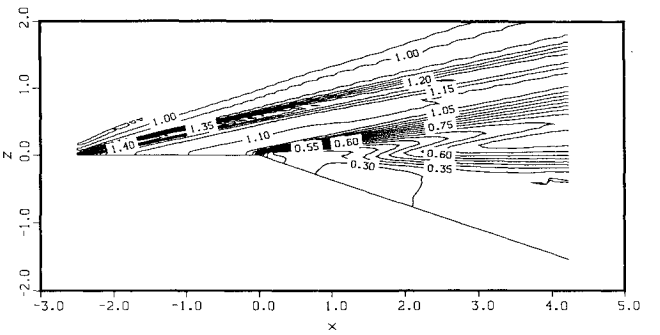

b) Fine grid ($129 \times 97 \times 129$)

Fig. 9 Comparison of grid refinement (center plane pressure contours).

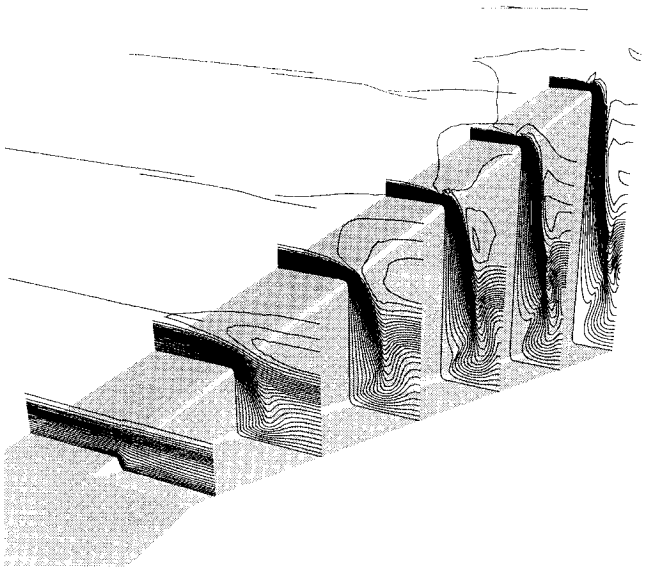

Fig. 10 Mach number contours (adiabatic).

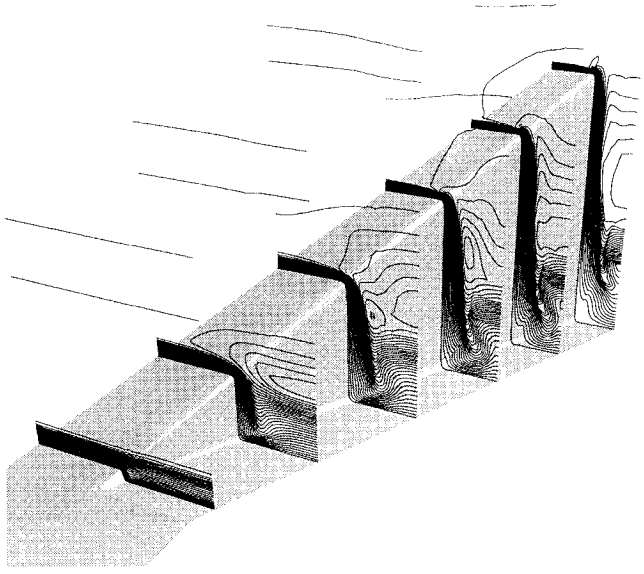

Fig. 11 Mach number contours (isothermal).

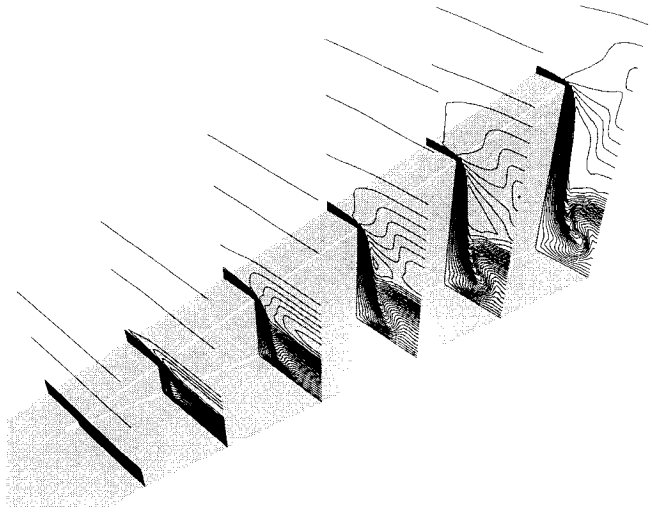

Fig. 12 Mach number contours for wide slot.

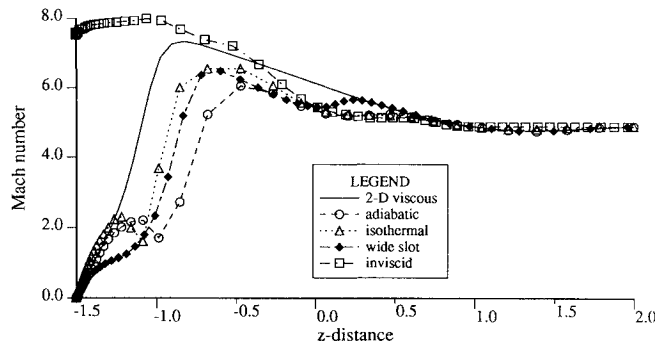

a) Mach number

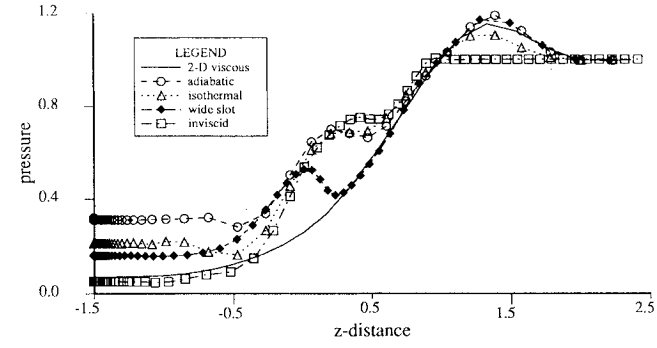

b) Pressure

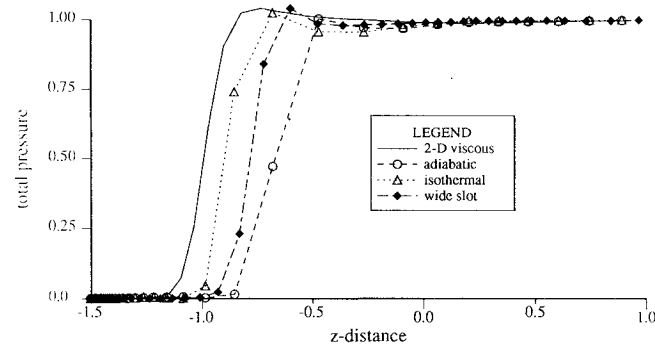

c) Total pressure

Fig. 13 Comparison of flow profiles at the exit center.

Prandtl-Meyer flow over the two-dimensional geometry. For a fixed freestream Mach number, based on the two-dimensional inviscid Prandtl-Meyer expansion, the mass flux induced in the slot at first increases as the wedge angle increases. As the wedge angle reaches the limit such that the last ray of its Prandtl-Meyer expansion fan, emanating from the corner, becomes parallel to the incoming flow (along the top edge of the slot), the mass flux through the slot reaches a constant. Any further increase of expansion wedge angle after that will only expand the flow in the slot further but not increase the total amount of mass flux through the slot. (For a Mach 4.9 flow, the limiting wedge angle for constant mass flux is about 9.5 deg, with a corresponding peak Mach number of about 6.08.) The effective expansion angles for the present study, both two-dimensional and three-dimensional cases, are larger than the limiting angle. Hence, the mass flux is not significantly affected by the viscous blockage. (Note that the adiabatic narrow case is close to the limit.) We observed that, in the present calculations, the mass flux is mainly contributed by the flow in the upper portion of the slot $-0.5 \lesssim z \lesssim 0$ in Fig. 13. (The flows in the upper portion of the slot are not very much different since their effective angles are large

Table 2 3-D calculated results at exit plane ($x = 4.2$)

	adiabatic	isothermal	wide	3-D Inviscid
p/p_∞ min	0.283	0.164	0.130	0.046
Mach No. max	6.06	6.56	6.59	8.03
Effective Angle	9.3°	12.5°	12.7°	19.7°
mass flux	0.1846	0.2014	0.1932	0.2206
p_t loss	0.736	0.598	0.592	0.052

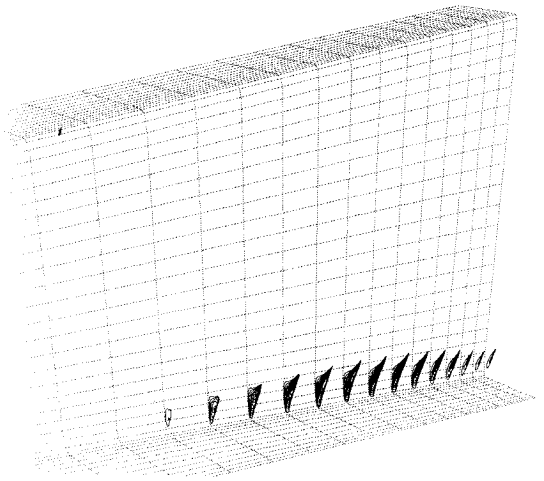

Fig. 14 Contours of negative streamwise velocity.

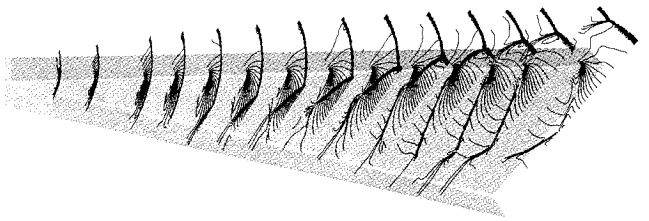

Fig. 15 Pressure contours for compression slot (inviscid)

enough as discussed above.) The lower portion of the slot ($z \lesssim -0.5$) mainly contains a layer of highly expanded low-density fluid and hence contributes very little mass flux. Another point is that, in the three-dimensional case, the expansion around the axial corner induces cross flow that results in a higher mass flux than in the two-dimensional solutions.

As mentioned before, the enhancement of mass flux due to cross flow leads to an adverse pressure gradient. For the narrow slot cases, this actually resulted in a small region of reversed flow. Figure 14 shows contours of negative streamwise velocity for the adiabatic narrow slot case. Note that this flow reversal is confined to a small region near the juncture of the slot bottom with the vertical wall. The isothermal case exhibited roughly the same behavior. The wide-slot calculation showed no flow reversal.

As a final case, we show Mach number contours for a preliminary calculation carried out for an inviscid 20 deg compression ramp. In this case, many shock waves are present and TVD flux limiting is used. Figure 15 shows Mach contours at several ($y - z$) planes. The wave generated from the axial corner now has a more dominant effect on the flow in the slot. The shock generated at the compression ramp is initially curved. The shock eventually reflects back and forth in the slot, and by the time it reaches the exit plane, the outer shock is almost straight, covering both the ramp and the slot. Since the real scramjet design utilizes both expansion and compression processes, the compression case needs to be studied in detail.

V. Concluding Remarks

The compressible Navier-Stokes equations are solved numerically for hypersonic flow over a three-dimensional ramp with a narrow expansion slot. The purpose of a compression ramp with an expansion slot is primarily to induce high momentum fluid through the slot to enhance mixing with the injected fuel. The computational results show that the viscosity plays an important role in the expansion process of hypersonic flow over a narrow slot. The boundary layer thickens so much that the effectiveness of expansion is substantially reduced. Cases with various wall temperatures and slot widths are studied. Calculations show that wall cooling reduces the thickness of the boundary layer and hence increases the flow expansion. The mass flux is primarily contributed from the upper portion of the slot. In the lower portion of the slot, inviscidly, the flow is dominated by a highly expanded low-density fluid, and viscously, by a viscous layer. As a direct consequence, as soon as the wedge angle is large enough, the mass flux through the slot is not affected significantly. There exists a limit mass flux rate for a two-dimensional flow with fixed incoming Mach number over a simple expansion corner. The three-dimensional viscous solutions exhibit cross flow expansion along the axial corner that results in higher mass fluxes than the two-dimensional solutions.

References

[1]Waltrup, P. J., "Hypersonic Airbreathing Propulsion: Evolution and Opportunities," AGARD Conference Proceedings of Aerodynamics of Hypersonic Lifting Vehicles, AGARD-CP-428, Paper 12, April 1987.

[2]Cordova, J. Q. and Barth, T. J., "Grid Generation for General Two-dimensional Regions Using Hyperbolic Equations," AIAA Paper 88-0520, Reno, NV, Jan. 1988.

[3]Pulliam, T. H. and Steger, J. L., "Recent Improvements in Efficiency, Accuracy, and Convergence for Implicit Approximate Factorization Algorithms," AIAA Paper 85-0360, Reno, NV, Jan. 1985.

[4]Beam, R. and Warming, R. F., "An Implicit Finite-Difference Algorithm for Hyperbolic Systems in Conservation Law Form," *Journal of Computational Physics*, Vol. 22, Sept. 1976, pp. 87-110.

[5]Van Leer, B., "Upwind-Difference Methods for Aerodynamic Problems Governed by the Euler Equations," *Lecture Notes in Applied Mathematics*, Vol. 22, 1985.

[6]Thomas, J. L., van Leer, B., and Walters, R. W., "Implicit Flux-Split Schemes for the Euler Equations," AIAA Paper 85-1680, July 1985.